Experimental investigation of a rotating drum heat exchanger for latent heat storage

Jonas Tombrink, Henning Jockenhöfer, Dan Bauer

German Aerospace Center (DLR), Institute of Engineering Thermodynamics

Pfaffenwaldring 38-40, 70569 Stuttgart, Germany

Phone: +49-711-6862-8835, e-mail: jonas.tombrink@dlr.de

Abstract

With latent heat thermal energy storages, thermal energy can be stored at a constant temperature level with high storage density using the enthalpy of the solid-liquid phase change of a material. During the discharge process of a latent heat thermal energy storage, phase change material (PCM) solidifies at the heat transfer surface and increases the thermal resistance. This decreases the transferred thermal power with time and the state of charge. The rotating drum heat exchanger, experimentally investigated in detail for the first time in this paper, overcomes this limitation by removing the PCM layer. While a heat transfer fluid passes through the inside of the rotating drum, which is partially immersed in liquid PCM, the PCM solidifies at the outer side. The solidified layer is removed at each rotation by a fixed scraper. Thus, the layer thickness and the thermal power are kept constant over time. The solidified PCM can be stored separately from the liquid phase, resulting in a complete independence of thermal power and storage capacity. A commissioned experimental test rig using a low temperature PCM is used for the investigation of the heat transfer potential, the layer thicknesses, the mechanical energy needed for the removal of the solidified layer and as a proof of concept. The experimental data show a consistent heat transfer which is increasing for higher rotational speeds. With the presented test rig, the heat transfer density is up to 6.8 $kW \cdot m^{-2}$ based on the total drums shell surface of the rotating drum at a temperature difference of 5 K between the melting point of the PCM and the temperature of the heat transfer. Adhering liquid PCM increases the total heat transfer by up to 60 % as the liquid PCM solidifies also after the surface left the liquid PCM. While the measured solidified layer decreases to below 0.05 mm with higher rotational speeds, the adhering layer is slightly increasing. The results show the high potential of the rotating drum heat exchanger concept for the generation of steam out of a high temperature PCM.

Keywords:

Active Latent Heat Thermal Energy Storage; Rotating Drum; Scraped Heat Exchanger; Phase Change Material; Solidification; Adhesion

Highlights

- Experimental study of a rotating drum heat exchanger for latent heat storage
- Investigation of heat transfer, layer thicknesses and required mechanical energy
- Constant and fully controllable heat transfer during the discharge process
- Complete separation of power and capacity achievable
- Measured heat transfer of up to 6.8 $kW \cdot m^{-2}$ based on the total drum shell surface

Nomenclature

Latin Symbols

c_p	heat capacity at constant pressure ($J \cdot kg^{-1} \cdot K^{-1}$)
$\dot{m}$	mass flow ($kg \cdot s^{-1}$)
n	rotational speed (min^{-1})
P	(electrical-) power (W)
p	pressure (Pa)
$\dot{Q}$	heat flow (W)
s	thickness (m)
T	temperature (K)
t	time (s)
x	length (m)

Greek Symbols

α	heat transfer coefficient ($W \cdot m^{-2} \cdot K^{-1}$)
Δh	heat of fusion of the PCM ($J \cdot kg^{-1}$)
ΔT	temperature difference (K)
η	dynamic viscosity (Pa·s)
Θ	immerging angle (°)
λ	thermal conductivity ($W \cdot m^{-1} \cdot K^{-1}$)
ϱ	density ($kg \cdot m^{-3}$)

Subscripts/Abbreviations

PCM	Phase Change Material
HTF	Heat Transfer Fluid
m	melting
l	liquid
s	solid
char	charge
dischar	discharge

Further Abbreviations

LHTES	Latent Heat Thermal Energy Storage
PCM	Phase Change Material

1 Introduction

For the transition of the energy system from limitedly available and carbon dioxide emitting fossil fuel consumption towards the usage of fluctuating renewable energy, the demand of energy needs to be decoupled from its production. This can be achieved by using suitable energy storage systems. Renewable energy from solar and wind will be available primarily in form of electricity. However, the pure demand of thermal energy in industrial applications for process heat in the temperature range of 100 to 400 °C in the EU28 member states amounts to around 2200 PJ per year, which is around 5 % of the total final energy consumption throughout all sectors [1]. Storing the energy in form of the required thermal energy offers advantages regarding the limited availability of critical resources for electrochemical energy storages and cost savings. Apart from that, there is the possibility to convert electricity from stored thermal energy by using a suitable thermodynamic cycle [2].

Latent heat thermal energy storages (LHTES) utilize the phase change enthalpy, usually between liquid and solid state, of the storage material (phase change material, PCM). Their essential characteristic is the isothermal temperature level during the melting (charging) and solidification (discharging) process. In applications that include isothermal processes, the required temperature difference for the heat transfer can be kept constant or minimized for an increased exergetic efficiency of the storage system. This includes the supply of process steam with specific requirements for industrial applications as well as the supply of organic- or water steam for electricity production. The exergetic efficiency is further maximized by an isothermal charging process e.g. by a condensing fluid (Figure 1). By overheating the liquid PCM above its melting point or subcooling the solid PCM below its solidification temperature, the sensible heat of the PCM can be used for energy storage as well. This increases the storage density and decreses the specific costs of the storage material simultaneously. For the generation of steam in a temperature range between 150 °C and 350 °C, nitrate salts are well suited. Especially sodium nitrate is cost attractive and has an abundant availabillity [3]. However, these materials have a limited thermal conductivity. During the discharge process, liquid PCM is solidifing at the cooled heat exchanger surface and a solidified PCM layer is growing. The phase change enthalpy released during the phase change is emitted at the boundary between solid and liquid PCM as shown in Figure 2. Thus, the thermal energy has to be transferred through the growing solidified layer. This causes a decline of the heat transfer capability during the discharge process with time and state of discharge. During the charging process of a LHTES the solidified PCM layer is melted at the heat exchanger surface. The heat transfer from the liquid PCM to the heat exchanger surface is increased by natural convection [4, 5] and can be further increased by forced convection. Therefore, most activities to improve LHTES are focusing on the discharge process as is the case in this work.

To overcome the discharge limitation, extensive reaserch has been conducted on so called passive LHTES. Among others, the mainly used basic principles are to increase the effective heat transfer surface or to increase the effective thermal conductivity of the PCM. The effective heat transfer

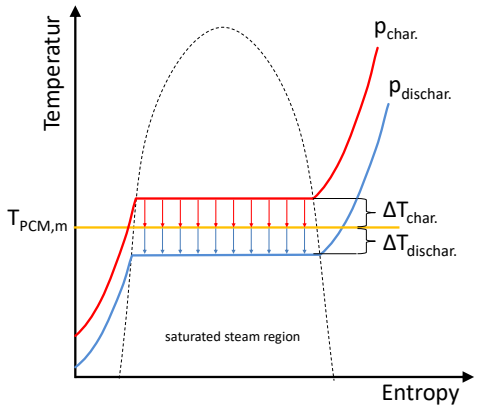

Figure 1: Constant temperature difference during charging and discharging of a PCM-Storage

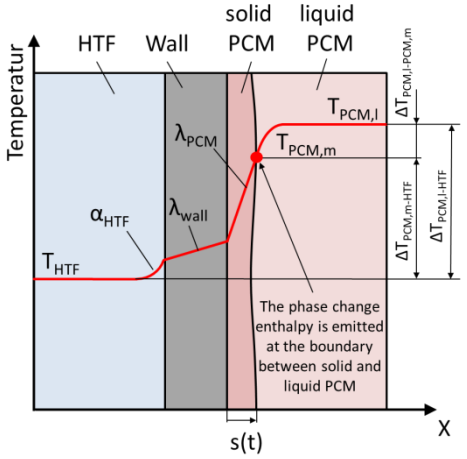

Figure 2: Temperature profile of a heat exchanger between a HTF and solidifying PCM

can be increased by integrating a heat transfer structure in the PCM [6-9] or a macro-encapsulation of the PCM [10]. The effective thermal conductivity can be increased by modifying the PCMs thermal properties e.g. by incorporating of nanoparticles [11, 12], micro-encapsulation [13, 14] or compression of the PCM to a composite [15]. However, the thermal power and thermal capacity of conventional passive LHTES with fixed heat exchangers and non-moving PCM is defined by its design at a certain ratio. Thus, if the capacity is enlarged, the heat transfer structure has to be incresed as well. This limits possible cost savings due to scaling effects especially for large long-time storages. Another possibility to overcome the limited heat transfer potential of available low cost PCMs is the use of active LHTES. Here, an active motion transports the PCM. This results in a constant heat transfer as the solidified layer thickness is kept constant in average. Beside the rotating drum firstly introduced in [16] and discussed in detail in this paper, further concepts of active LHTES have been published. Among others, these are mainly:

- The Screw-Heat-Exchanger concept, in which two parallel screws, known from the plastic extrusion, are transporting the PCM and serve as heat exchanger [17].
- In the PCM-Flux concept, PCM is moved in a container linearly over a locally fixed heat exchanger [18].
- In [19], a plate heat exchanger is presented, whose heat transfer surface is periodically scraped off by a linearly moving scraper.
- A vertically rotating, scraped rotating drum with PCM around the drum in a closed enclosure is presented in [20].

All of these concepts have been demonstrated experimentally on an experimental scale. However, all of them have in common, that there is a layer thickness of solid PCM given at the heat exchanger surface, which dominates the heat transfer. Further concepts of scraped surface heat exchangers are mainly optimized for the process of freezing or for the increase of the convective heat transfer without solidification [21-24]. Within Figure 3, the thermal resistances of a typical heat transfer problem of latent heat storages are given. The solidified PCM layer clearly dominates the heat transfer resistance if it is thicker than 0.1 m. Only with a further reduction of the solidified PCM layer thickness the thermal resistances of the steel wall and the evaporating water become dominant.

The novel concept of the rotating drum heat exchanger is designed from scratch to minimize the layer thickness of the solid PCM and thus maximize the surface specific heat transfer of the heat exchanger. Furthermore, a separation of the solidified PCM from the liquid PCM is a key element for the separation of power and capacity. The basic concept of the rotating drum heat exchanger is shown in Figure 4. A rotating drum is partially immersed into liquid PCM. An evaporating fluid extracts thermal energy while passing the inside surface of the heat transfer wall. Simultaneously, liquid PCM releases its phase change enthalpy during solidification at the outer surface of the wall. To maintain a minimum thickness of the solidified PCM layer, a fixed scraper removes the layer with each rotation. The scraped PCM can be stored separately from the liquid PCM. This leads to a complete separation

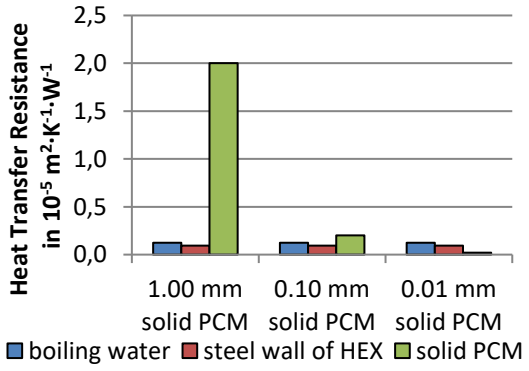

Figure 3: Typical values for the thermal resistances of the heat transfer network shown in Figure 2 for boiling water (α = 8000 W·m^{-2}·K^{-1}), boiler steel wall (λ = 54 W·m^{-1}·K^{-1}, s = 5 mm) and sodium nitrate as PCM (λ = 0.5 W·m^{-1}·K^{-1})

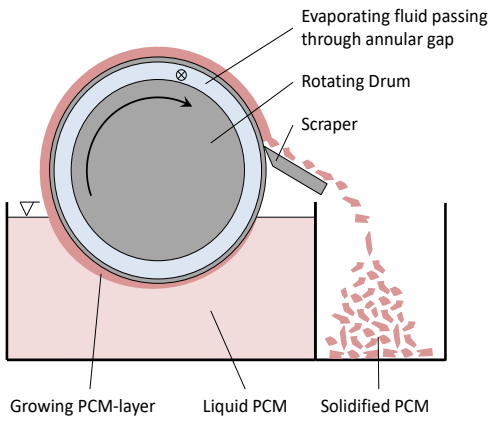

Figure 4: Principle of the rotating drum heat exchanger

of the thermal power that can be transferred and the thermal energy that can be stored with the thermal energy storage system. The separation leads to cost savings for medium and long-term storages with high storage capacities, since the heat exchanger as the main part of the storage system can be chosen independently in its size. The transferred thermal energy can be controlled by the rotational speed. This leads to a flexible system for the provision of changing steam requirements. The overall specific thermal energy density of the storage material can be increased by extending the temperature range used above and below its phase change temperature. Thus, the energy density is composed of the latent heat of the phase change and the sensible heat stored in both the liquid and the solid phase of the storage material. The maximum temperature of the liquid PCM is limited by the decomposing temperature of the PCM or the material specific maximum operating temperature of the rotating drum and its components.

Within this paper, the concept of the rotating drum heat exchanger for latent heat storage is examined experimentally in detail for the first time. Therefore, an experimental test rig using a low-temperature PCM is commissioned. The use of a low-temperature PCM allows a more detailed investigation of the various effects while the basic physical properties of the heat transfer remain unchanged compared to a high temperature system. The methodology of the experimental investigation is described in the following section. The main objective of the research is a proof of concept and to identify the technologies potential regarding the heat transfer. Furthermore, the influence of different effects such as adhesion and different temperature differences are examined.

2 Experimental Details

The experiments aim is a proof of the concept and an examination of its heat transfer potential. Furthermore, the layer thickness, the adhering liquid PCM and the mechanical energy required to remove the solidified PCM are determined. The experimental test rig is introduced in the following section. Liquid water is used as HTF and the low temperature PCM decanoic acid is used for a detailed examination of the heat transfer.

2.1 Overall design of the experimental test rig

The main part of the experimental test rig is a rotating steel drum which serves as the heat exchanger. The design and the geometrical properties of the rotating drum are given in Figure 5. It is made out of pressure vessel steel P235GH with a thermal conductivity of 54 $W \cdot m^{-1} \cdot K^{-1}$. The rotating drum is integrated into a test rig whose piping and instrumentation diagram is shown in Figure 6. A water circuit flows through the rotating drum with a high mass flow rate ($\dot{m}_1$) of 1.2 $kg \cdot s^{-1}$. The mass flow of flow of water is provided by a submersible pump. This decreases the temperature difference of the water between the inlet (T_1) and the outlet (T_2) of the drum to below 1 K to reach an almost isothermal process along the rotating drum. Furthermore, the annular gap inside the rotating drum increases the flow velocity of the water to 1.1 $m \cdot s^{-1}$ which results in an increased convective heat transfer between the steel drum and the water. The convective heat transfer coefficient can be estimated to 4176 $W \cdot m^{-2} \cdot K^{-1}$ according to [25]. The water circuit is cooled by a thermal oil circuit with a plate heat

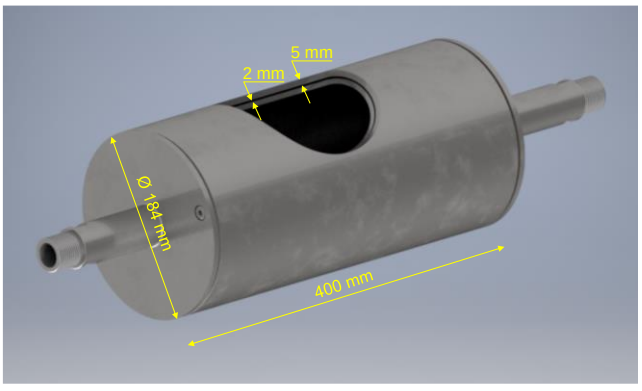

Figure 5: Geometrical properties of the rotating drum

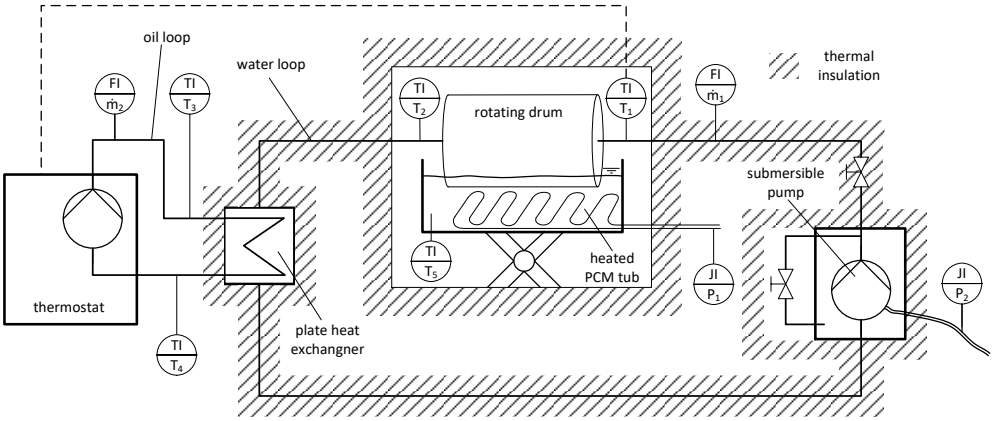

Figure 6: Piping and instrumentation diagram of the test rig

exchanger. The thermal oil circuit is cooled by a commercial thermostat which is controlled by the drums inlet temperature (T_1). The PCM is located in a tub below the rotating drum. The PCM is melted and heated by electrical heating elements inside the tub by direct contact. The tub can be lifted by a laboratory lift mounted below the tub to immerse the drum into the PCM. The rotating drum is connected to the water circuit via rotary unions supported by rotating bearings. It is driven by a stepper motor and a belt drive. The rotational speed is continuously adjustable in the range of 0-30 min^{-1}. The scraper is made of a 0.5 mm stainless steel sheet, which is tangentially pressed against the drums surface by its internal elasticity. The solidified and scraped PCM falls back into the liquid PCM tub and is re-melted by the electrical heater. This keeps the level of the PCM constant during operation. The entire water circuit is thermally insulated as well as the PCM tub and the rotating drum. Figure 7 shows a picture of the rotating drum for different rotational speeds. Figure 8 shows the entire test rig.

a) b)

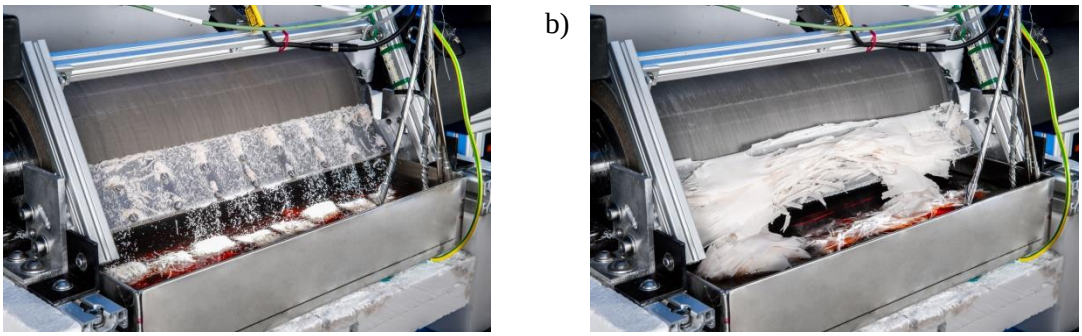

Figure 7: Picture of the rotating drum during operation (a), a) at 6 min^{-1}, b) at 12 min^{-1}

Figure 8: Photo of the experimental test rig

2.2 Phase Change Material

The use of unpressurised water as HTF requires a PCM with a phase change temperature in the range of 0 – 100 °C. In the temperature range between 20 and 75°C, fatty acids have been prooven as suitable phase change materials [26-28]. For the solidification, the temperature of the water in the water circuit is cooled up to 10 K below the melting temperature of the PCM. To reduce its heat losses a melting point of 10 K above the ambient temperature of 22 °C is preferable. Decanoic acid, also referred to as capric acid, is selected as the PCM. The melting point is 31.5 °C [29]. It is available in high purity, non-toxic and suitable as PCM for low temperature applications [27, 28]. Table 1 shows the material properties of decanoic acid.

Table 1: Thermophysical properties of decanoic acid

Description	Variable	Value	Unit	Remark	Source
Melting point	$T_{PCM,m}$	31.5	°C		[29]
Phase change enthalpy	Δh_{PCM}	153	$kJ \cdot kg^{-1}$		[29]
Thermal conductivity, liquid	$\lambda_{PCM,l}$	0.149	$W \cdot m^{-1} \cdot K^{-1}$	(at 40 °C)	[29]
Thermal conductivity, solid	$\lambda_{PCM,s}$	0.204	$W \cdot m^{-1} \cdot K^{-1}$	(at 20 °C)	[28]
Density, liquid	$\varrho_{PCM,l}$	886.3	$kg \cdot m^{-3}$	(at 37,8 °C)	[30]
Density, solid	$\varrho_{PCM,s}$	850	$kg \cdot m^{-3}$	(at 25 °C)	[28]
Viscosity	$\eta_{PCM,l}$	0.00633	Pa·s	(at 37,8 °C)	[31]
Heat capacity, liquid	$c_{p,PCM,l}$	2.0883	$kJ \cdot kg^{-1} \cdot K^{-1}$	(at 35-65°C)	[32]
Heat capacity, solid	$c_{p,PCM,s}$	2.0967	$kJ \cdot kg^{-1} \cdot K^{-1}$	(at 0-24 °C)	[32]

2.3 Measurement of the heat transfer

A small to zero temperature difference between the inlet (T_1) and the outlet (T_2) temperature of the rotating drum is aspired for a homogeneous heat transfer at the drum surface. By doing so, it is not possible to measure the transferred heat of the rotating drum directly by measuring the temperature difference between the inlet (T_1) and the outlet (T_2). Therefore, the heat transfer of the rotating drum is calculated by the energy balance of the entire water circuit.

The energy transferred by the plate heat exchanger to the water circuit can be determined with the specific heat capacity of the thermal oil $c_{p,l,oil}$, by measuring the temperature difference between inlet (T_3) and outlet (T_4) of the plate heat exchanger and the mass flow ($\dot{m}_2$) of the thermal oil, pumped through the oil circuit. The mass flow ($\dot{m}_2$) of the oil circuit is adjustable between 0.055 $kg \cdot s^{-1}$ and 0.18 $kg \cdot s^{-1}$, which is low compared to the mass flow in the water circuit ($\dot{m}_1$). This leads to an increased temperature difference between the inlet (T_3) and the outlet (T_4) of the thermal oil at the plate heat exchanger. The temperature difference of the thermal oil depends on the mass flow ($\dot{m}_2$) as well as the thermal power of the rotating drum and is in the range of 3 K up to 10 K. Since the efficiency of the used pump is unknown, a submersible pump is used. Thus, the total amount of electrical energy is dissipated to the water circuit, measured with an electrical power meter (P_2). As a result of this, the heat transferred at a steady state at the rotating drum surface is the difference between the heat extracted by the plate heat exchanger and the heat dissipated by the pump as given in equation (1):

$$\dot{Q}_{RD} = \dot{m}_2 \cdot c_{p,Oil,l}\left(\overline{T_{3,4}}\right) \cdot (T_4 - T_3) - P_2$$

The electrical energy P_1 needed to re-melt and heat the PCM in the tub is also measured by a power meter. For an ideal system with no heat losses to the ambient air and neglecting the mechanical energy transferred into the system by the stepper motor, it must apply

$$\dot{Q}_{RD} = P_1.$$

The figures in section 3.1 show P_1. The heat losses and the mechanical energy needed for scrapping off the solidified PCM are discussed in section 3.3 by comparing $\dot{Q}_{RD}$ and P_1.

2.4 Measurement of the layer thickness of the solid PCM

The layer thickness of the solidified PCM after the surface emerges from the liquid PCM is measured by a triangular laser distance measurement device (Type IL-S025 produced by KEYENCE). It is located shortly before the solidified layer is scraped off by the scraper and the surface is re-emerged into the liquid PCM again as shown in Figure 9 a) and b). The laser device is always measuring the distance to the PCM surface only. The layer thickness can be determined by comparing the measured distance with solidified PCM and the measured distance to the bare surface of the drum.

2.5 Experimental methodology

In the beginning of each experiment, the PCM is melted by the electrical heaters and heated to $T_{PCM,l}$. The electrical heaters are controlled by thermocouples inside the PCM. Since there is no temperature change during the phase change, the temperature of the liquid PCM $T_{PCM,l}$ has to be above the melting point because the thermocouples cannot detect the phase state of the PCM at the melting temperature. The HTF inlet temperature of the rotating drum T_1 is set to a certain value and the rotation of the drum is started. Afterwards, the immersion depth is adjusted to 24 mm, considering the displacement of liquid PCM. This corresponds to an immersion angle Θ of 85°, which is equivalent to 24% of the total shell surface of the drum. The total immerged drum shell surface is therefore 0.054 m^2. The nomenclature of the experiments consists of three figures, the total temperature difference between the liquid PCM and the HTF ($\Delta T_{PCM,l\text{-}HTF}$), the temperature difference of the solidification between the melting point of the PCM and the HTF ($\Delta T_{PCM,m\text{-}HTF}$) and the temperature difference between the liquid PCM and the melting point of the PCM ($\Delta T_{PCM,l\text{-}PCM,m}$). The temperature configuration is illustrated in Figure 2 as well. Each temperature configuration was examined for different rotational speeds between 0.25 min^{-1} and 25 min^{-1}. As the thermal power of the thermostat used is limited to 2.2 kW and the submersible pump dissipates 0.5 kW into the HTF circuit, the maximum power that can be measured at the rotating drum is 1.7 kW. The experiments are conducted for all three operation modes shown and discussed in section 0. Table 2 shows the measured temperature configurations and the nomenclature of the experiments. For a temperature of the HTF above the melting temperature of the PCM, no solidification occurs. Therefore, the temperatures differences to the PCM melting temperature $\Delta T_{PCM,m\text{-}HTF}$ and $\Delta T_{PCM,l\text{-}PCM,m}$ of the first five temperature settings given in Table 2 are not relevant. The data are measured after reaching a stationary HTF in- and outlet temperature and are recorded every second. The given data in section 4 shows the average values during the stationary operation.

Table 2: Measurement matrix of the temperature configurations and the nomenclature of the conducted experiments

$T_{PCM,m}$	T_{HTF}	$T_{PCM,l}$	$\Delta T_{PCM,l\text{-}HTF} = T_{PCM,l} - T_{HTF}$	$\Delta T_{PCM,m\text{-}HTF} = T_{PCM,m} - T_{HTF}$	$\Delta T_{PCM,l\text{-}PCM,m} = T_{PCM,l} - T_{PCM,m}$	Nomenclature = $\Delta T_{PCM,l\text{-}HTF}/\Delta T_{HTF\text{-}PCM,m}/\Delta T_{PCM,l\text{-}PCM,m}$
31.5 °C	34 °C	34 °C	0 K	-	-	**0K/-/ -**
		39 °C	5 K	-	-	**5K/-/ -**
		44 °C	10 K	-	-	**10K/-/ -**
		49 °C	15 K	-	-	**15K/-/ -**
		54 °C	20 K	-	-	**20K/-/ -**
	26.5 °C	36.5 °C	10 K	5 K	5 K	**10K/5K/5K**
		41.5 °C	15 K	5 K	10 K	**15K/5K/10K**
		46.5 °C	20 K	5 K	15 K	**20K/5K/15K**
		51.5 °C	30 K	5 K	25 K	**30K/5K/25K**
	21.5 °C	36.5 °C	15 K	10 K	5 K	**15K/10K/5K**
		41.5 °C	20 K	10 K	10 K	**20K/10K/10K**

2.6 Operational modes

For a detailed investigation of the influence of the different physical effect on the heat transfer, three different operation modes are defined as shown in Figure 9. When the drum surface emerges from the PCM bath, liquid PCM adheres to the solidified PCM layer. This adhering liquid PCM solidifies after the surface has left the liquid PCM and thus enlarges the active heat exchanger surface. With operation mode (a), the total heat transfer is measured including the additional heat transfer due to the solidification of the adhering PCM after the surface emerges from the liquid PCM. In operation mode (b), the adhering liquid is removed by a rubber lip mounted shortly after the surface emerges from the liquid PCM. Thus, the additional heat transfer from adhesion can be investigated by comparing the measured heat transfer of operation mode (a) and (b). The PCM, which solidifies at the heat exchanger surface, is cooled down below its melting point after the heat exchanger surface has left the liquid PCM. To investigate the amount of sensible heat transferred during this period, the entire PCM layer is

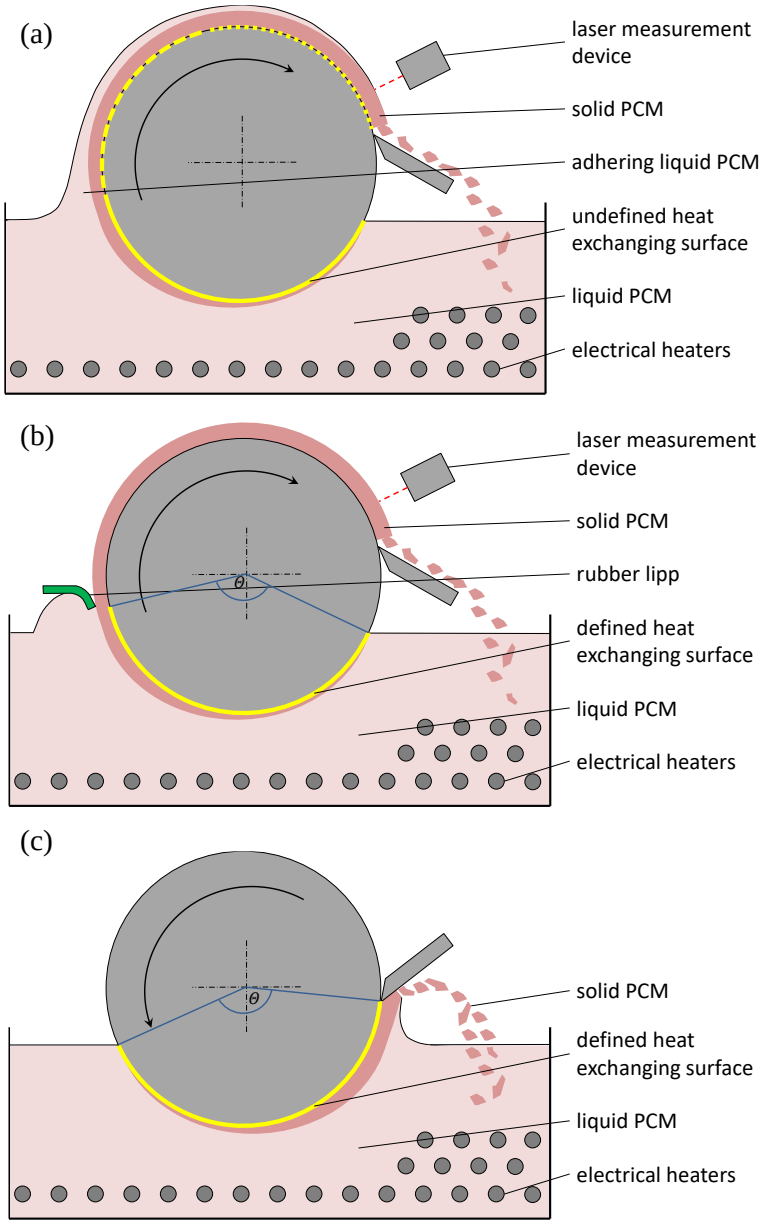

Figure 9: Examined mode of operation (a) scraping off the solidified layer and adhering layer shortly before re-immerge into liquid PCM (b) scraping off the solidified layer shortly before re-immerge, but removing the adhering liquid layer by a rubber lip shortly after the surface emerged the liquid PCM (c) scraping off the solidified layer shortly after the surface has emerged from the liquid PCM

removed shortly after the surface emerges from the liquid PCM in operation mode (c). This is done by reversing the direction of rotation and position of the scraper. As mentioned, the immerged drum shell surface is 0.054 m^2, which corresponds to the total active heat transfer surface during the operation mode (b) without adhesion. During the operation mode (c), the scraper can't be mounted directly at the emerging point of the drum due to constructive constraints. Therefore, adhering liquid PCM increases the active heat transfer surface to 0.067 m^2. For the measurements operation mode (a) with adhesion, the total drum shell surface is 0.19 m^2 from the point of immersion to the scraper. Here, the active heat exchanger surface is not exactly defined, as the adhering liquid PCM is completely solidified for low rotational speeds bevor it reaches the scraper. The total shells surface of the rotating drum is 0.23 m^2.

2.7 Uncertainty analysis

The directly applicable uncertainty of the power meter used to measure the heat transfer of the rotating drum is given as ± 2 %. The laser sensor which is used for the determination of the layer thickness has a linearity of 0.1 % and a repeatability of 1 µm. As both values are very low, no error bars are given in the figures in section 3. One has to consider that the overall uncertainty is depending of external reasons which are not able to quantify directly. First of all, the temperature of the liquid PCM is measured by several thermocouples within the liquid PCM with an uncertainty of 1.5 K. Furthermore, the immersion depth of the rotating drum is variating by ± 4 mm. As a result of this, the immersed shell surface is variating by ± 2 %. The repeatability for the heat transfer has been measured within pre-experiments where the heat transfer has been measured up to four times with the same configuration. The standard deviation calculated according to [33] is ± 54 W for the measured different rotational speeds between 0.25 min^{-1} and 15 min^{-1}.

3 Experimental results and discussion

The experimental data are shown and discussed in the following section. For the heat transfer at the rotating drum, the electrically measured data P_1 for heating the liquid PCM in the tub are presented. The heat transfer $\dot{Q}_{RD}$ is used for determining the heat losses and the mechanical power required for scraping the PCM off the drum. This is discussed in section 3.3.

3.1 Heat transfer at the rotating drum

The influence of the temperature configuration and the operational mode on the heat transfer will be discussed within this section. While the data of operation mode (b) and (c) are measured in the range from 0 min^{-1} to 25 min^{-1}, the data of operation mode (a) are only measured for lower rotational speeds due to the limited thermal power of the thermostat used, as described in section 2.5.

Convective heat transfer without solidification

By rotating the drum in liquid PCM with a HTF temperature $T_{PCM,l}$ above the melting temperature of the PCM, no solidification occurs. The measured data are given in Figure 10 for different rotational speeds and different temperature differences between the liquid PCM and the HTF. No data has been measured by using the rubber lip operation mode (b), as the heat transfer phenomena is the same as the operation mode (c). The progression of the heat transfer is almost linear. With higher rotational speeds the increase of the heat transfer flattens out slightly. So, the average increase of the data without adhesion is 27 W/min^{-1} in the range from 0 min^{-1} to 5 min^{-1} and 13 W/min^{-1} in the range from 20 min^{-1} to 25 min^{-1}. The heat transfer of the measurements with adhesion is higher than the heat transfer of the measurements without adhesion. While the measured heat transfer with adhesion exceeds the data without adhesion in average by 12 % at 2 min^{-1}, the increase is 10 % at a rotational speed of 10 min^{-1}. With no rotation, the shown heat transfer bases on natural convection of the liquid PCM. For no temperature difference between the liquid PCM and the HTF, the measured heat flow increases from 7 W at 0 min^{-1} to 29 W at 25 min^{-1}. This is explained by increasing heat losses to the ambient due to an increased circulation of the air inside the insulation.

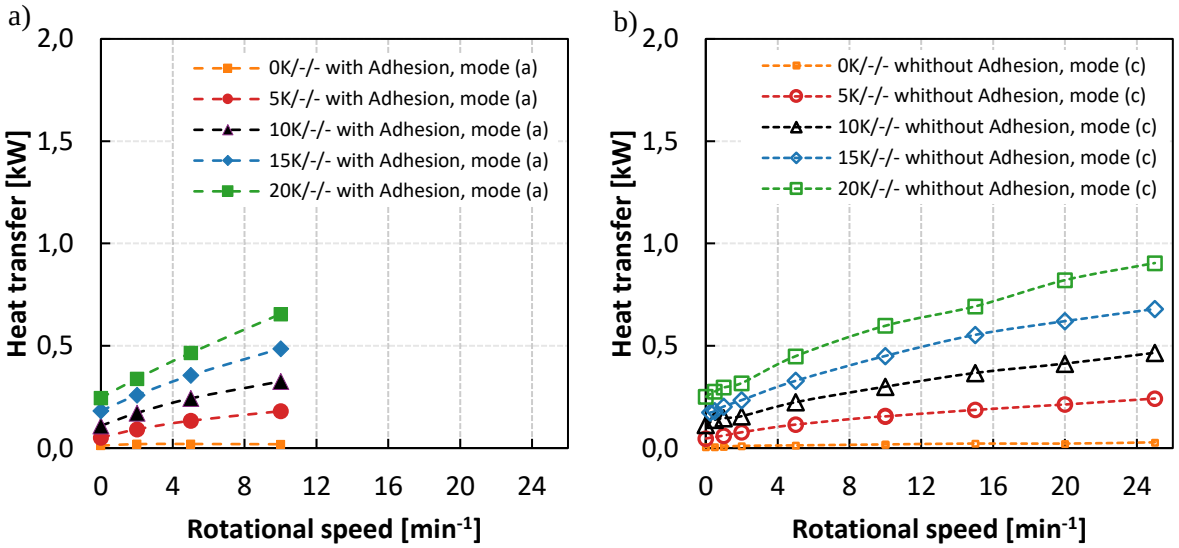

Figure 10: Measured heat transfer at the rotating drum for pure convective heat transfer without solidification a) with Adhesion b) without Adhesion

Influence of the temperature difference $\Delta T_{PCM,m\text{-}HTF}$

By decreasing the HTF temperature in the water circuit below the PCMs melting temperature, liquid PCM solidifies at the drums surface. In Figure 11 the measured heat transferred to the rotating drum is given for a common total temperature difference between the HTF and the liquid PCM temperature $\Delta T_{PCM,l\text{-}HTF}$ of 20 K. Thereby, the temperature difference between the HTF temperature and the melting temperature of the PCM $\Delta T_{PCM,m\text{-}HTF}$ is varied. The measurement of the heat transfer with solidification starts at a rotational speed of 0.25 min^{-1} as there are no stationary data available for no rotation. The heat transfer is increasing by an increase of $\Delta T_{PCM,m\text{-}HTF}$. So, doubling $\Delta T_{PCM,m\text{-}HTF}$ from 5 K to 10 K increases the heat transfer by 31 % in average. Compared to the measurements without solidification, the average increase of the heat transfer is 46 % for a $\Delta T_{PCM,m\text{-}HTF}$ of 5 K and 77 % for a $\Delta T_{PCM,m\text{-}HTF}$ of 10 K while the increase is higher for increasing rotational speeds. The increase of the heat transfer when increasing the rotational speed flattens out at higher rotational speeds. So, the average increase is 195 W/min^{-1} with adhesion and 180 W/min^{-1} without adhesion in the range between 0.25 min^{-1} to 2 min^{-1} compared to 96 W/min^{-1} with adhesion and 63 W/min^{-1} without adhesion when increasing the rotational speed from 5 min^{-1} to 8 min^{-1}. At rotational speeds below 0.5 min^{-1}, the pure convective heat transfer exceeds the heat transfer during solidification for these rotational speeds. This is a consequence of the reduced heat transfer through to the solidified PCM layer in comparison to purely convective heat transfer at the bare surface.

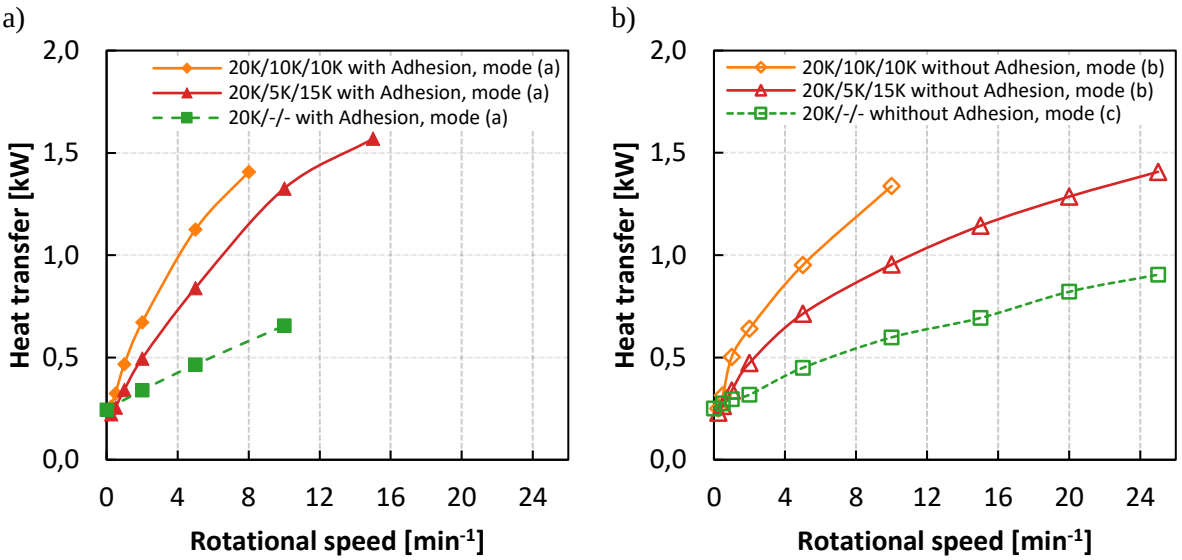

Figure 11: Measured heat transfer at the rotating drum at a common total temperature difference of 20 K and a variation of the temperature difference between the HTF and the PCM melting point a) with Adhesion, b) without Adhesion

Influence of the PCM temperature difference $\Delta T_{PCM,l\text{-}PCM,m}$

By increasing the temperature difference of the liquid PCM temperature and the melting temperature of the PCM $\Delta T_{PCM,l\text{-}PCM,m}$ at a constant temperature difference between the HTF and the melting temperature of the PCM $\Delta T_{PCM,m\text{-}HTF}$, the transferred heat is increased as shown in Figure 12. The average increase of the heat transfer is 7 % for an increase of $\Delta T_{PCM,l\text{-}PCM,m}$ from 10 K to 15 K and 28 % for an increase of $\Delta T_{PCM,l\text{-}PCM,m}$ from 15 K to 25 K. Thus, an increase of $\Delta T_{PCM,l\text{-}PCM,m}$ increases the heat transfer at the rotating drum significantly less than an increase of $\Delta T_{HTF\text{-}PCM,m}$. By an increasing rotational speed, the progression of the heat transfer flattens out as well. Thus, the average increase is 157 W/min^{-1} with adhesion and 139 W/min^{-1} without adhesion in the range between 0.25 min^{-1} to 2 min^{-1} compared to 51 W/min^{-1} with adhesion and 37 W/min^{-1} without adhesion when increasing the rotational speed from 10 min^{-1} to 13 min^{-1}.

Influence of the adhesion and the solidified PCM layer

The heat transfer at the rotating drum varies with the mode of operation (see Figure 9) as shown in Figure 13. The heat transfer is lowest when scraping off the adhering and solidified layer shortly after

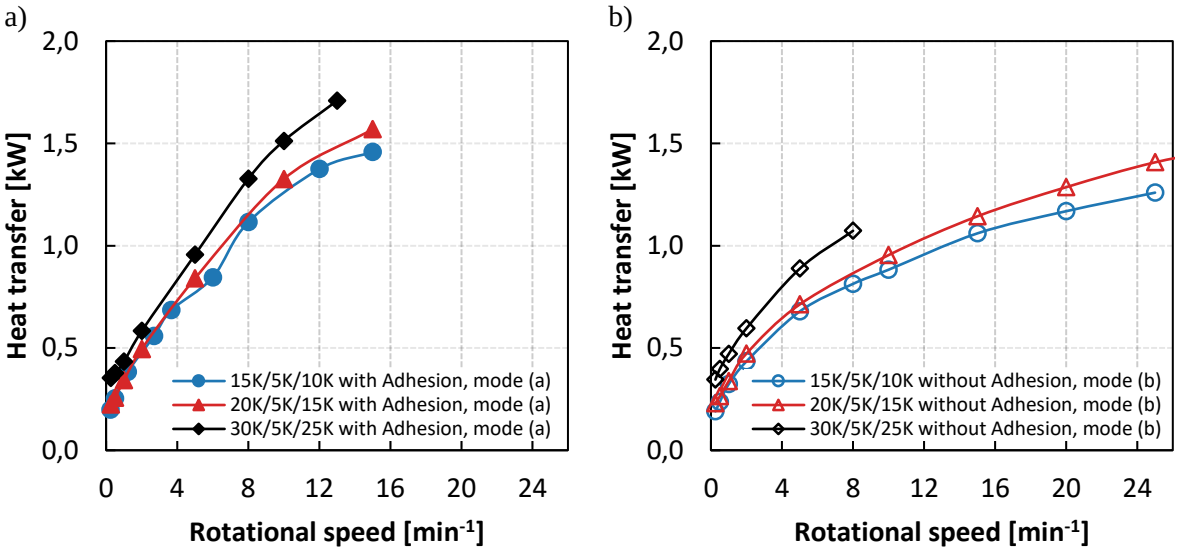

Figure 12: Measured heat transfer at the rotating drum at a common temperature difference between the HTF and the melting temperature of the PCM $\Delta T_{PCM,m\text{-}HTF}$ and a variation of the temperature difference between the HTF and the PCM melting point $\Delta T_{PCM,l\text{-}PCM,m}$ a) with Adhesion, b) without Adhesion

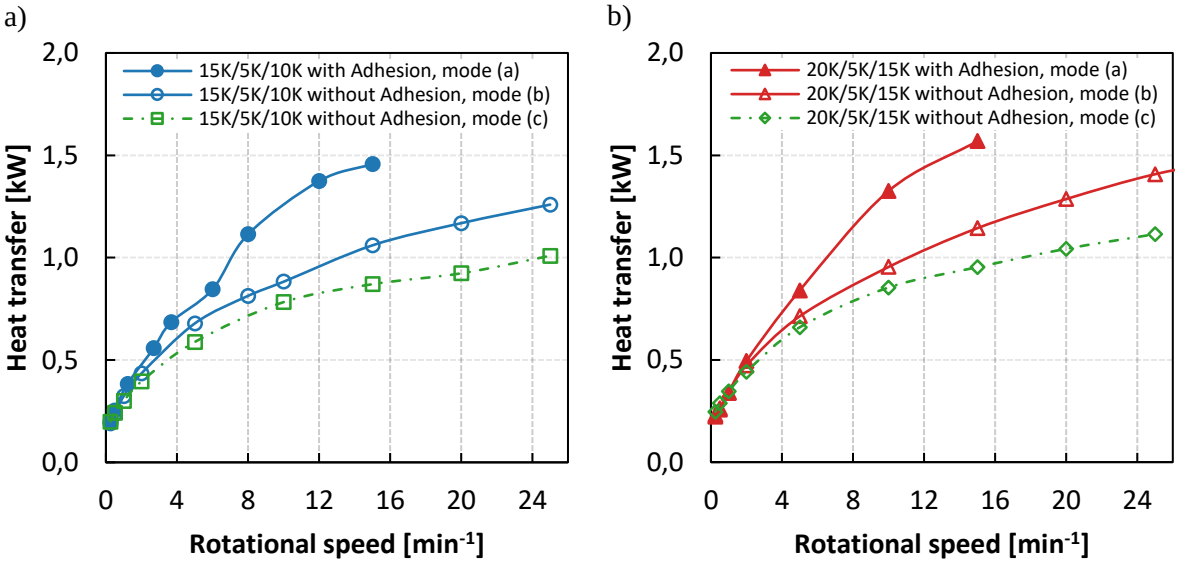

Figure 13: Measured heat transfer at the rotating drum for common temperature difference configuration of a) 15K/5K/10K and b) 20K/5K/15K and a variation of the operation mode (see Figure 9)

the drums surface emerges from the liquid PCM (operation mode (c)). The heat transfer is increased by 30 % in average when removing the adhering liquid layer shortly after the drums surface emerges from the liquid PCM, but scraping off the solidified PCM layer just before the surface re-immerses into the PCM (operation mode (b)). This increase is consistent for all rotational speeds. It can be explained in the way that the solidified layer is cooled below its melting point after the solid PCM has left the liquid PCM. Thus, the additional heat flow is the sensible heat within the solidified PCM layer. The adhering layer increases the heat transfer further by 45 % in average. This is because the active solidification surface of the rotating drum is enlarged as liquid PCM solidifies also after the surface has emerged the liquid PCM. Within the range of 0.25 min^{-1} and 10 min^{-1}, this increase of the additional heat transfer due to adhesion is increasing with higher rotational speeds. A further increase of the rotational speeds results in a consistent increase of 60 % in average for the rage between 10 min^{-1} and 15 min^{-1}. This is because the adhering liquid PCM is not totally solidified when it reaches the scraper for rotational speeds of 10 min^{-1} and above.

3.2 Layer thickness of PCM at the rotating drum

The layer thickness of the solidified PCM layer is measured with and without the influence of the adhesion (operation modes (a) and (b) in Figure 9). The additional layer thickness due to the adhesion can be determined by the difference of these both measurements. The experimental results are shown in Figure 14. The layer thickness varies with the temperature difference of both $\Delta T_{HTF\text{-}PCM,m}$ and $\Delta T_{PCM,l\text{-}PCM,m}$. By increasing $\Delta T_{PCM,m\text{-}HTF}$ from 5 K to 10 K at a constant total temperature difference $\Delta T_{PCM,l\text{-}HTF}$ of 20 K, the average total layer thicknesses is increased by a factor of 1.5 while the average

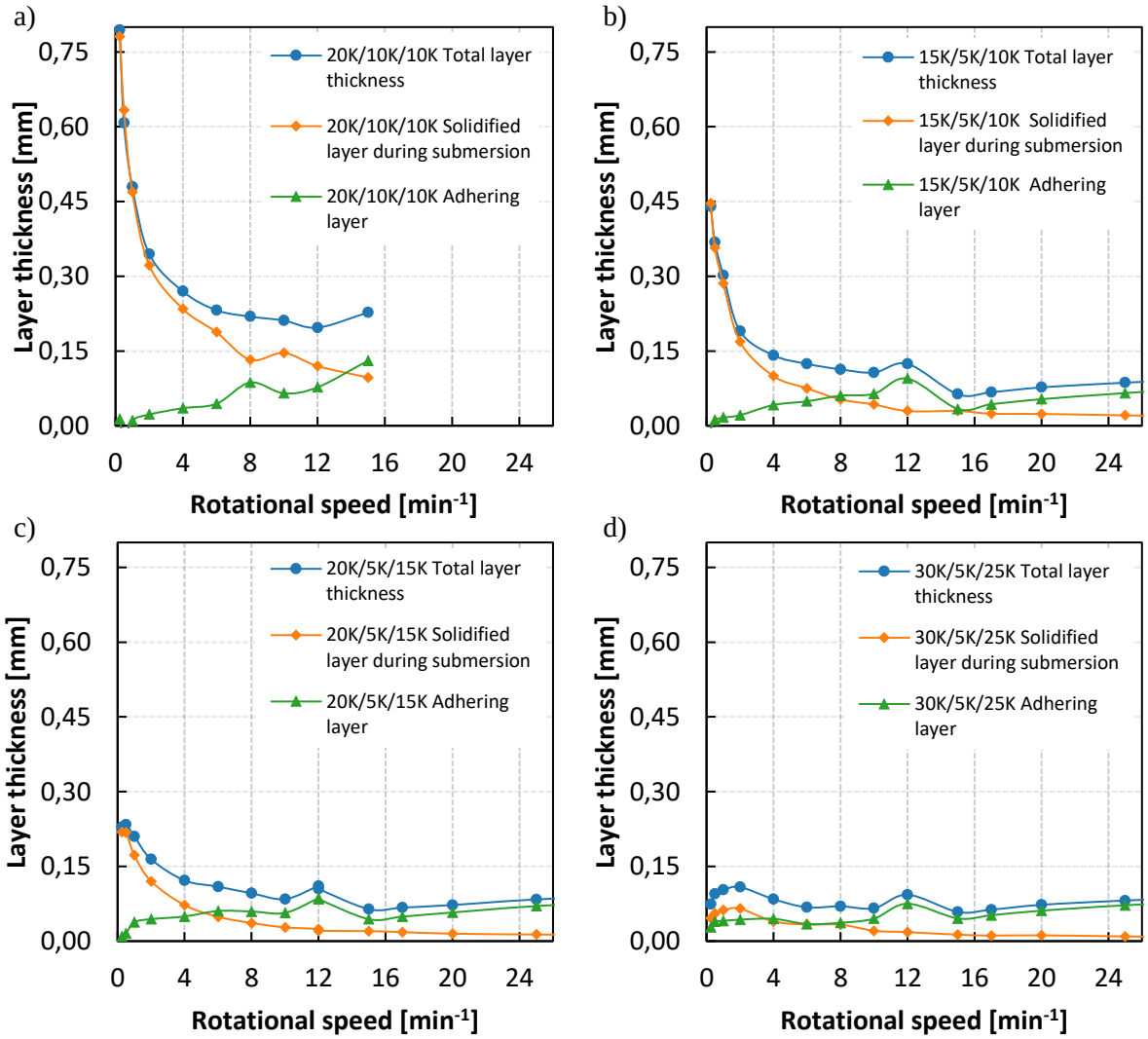

Figure 14: Measured total layer thicknesses, measured layer thicknesses during submersion and resulting calculated adhering layer thicknesses at the rotating drum surface for different temperature configurations

layer thickness without adhesion is increased by a factor of 2.7 in average. In the same way, the calculated adhering layer remains almost constant and is decreased by only 15 % in average. By increasing $\Delta T_{PCM,l\text{-}PCM,m}$ at constant $\Delta T_{PCM,m\text{-}HTF}$, the solidified PCM layers are decreased. So, the layer thickness without adhesion is decreased by 33 % in average when increasing $\Delta T_{PCM,l\text{-}PCM,m}$ from 10 K to 15 K and 40 % in average when increasing $\Delta T_{PCM,l\text{-}PCM,m}$ from 15 K to 25 K. The total layer thickness decreases at low rotational speeds more than at high rotational speeds. The average decrease is 24 % and 41 % for a change of $\Delta T_{PCM,l\text{-}PCM,m}$ from 10 K to 15 K and 15 K to 25 K at a rotational speed between 0.25 min^{-1} and 10 min^{-1} while the average decrease is only 4 % and 7 % at a rotational speed between 12 min^{-1} and 25 min^{-1}. The calculated adhering layer remains nearly unchanged over the whole range of the rotational speed for the same change in temperature. The average change is below 0.01 mm. The measured total layer thicknesses at a $\Delta T_{PCM,m\text{-}HTF}$ of 5 K have a local maximum at 12 min^{-1}. For rotational speeds of 12 min^{-1} and above, adhering liquid PCM is removed by the scraper together with the solidified PCM. At rotational speeds of 15 min^{-1} and more, the laser measuring device does not measure clear data. While it can be assumed that the solidified layer under the adherent liquid PCM decreases at higher rotational speeds, it can be assumed that the adherent liquid layer increases.

3.3 Mechanical power to remove the solidified PCM

By comparing the measured electrical power to re-melt and heat the PCM tub P_1 and the thermal power measured at the plate heat exchanger $\dot{Q}_{RD}$, the heat losses and the mechanical power needed to remove the solidified PCM from the drums surface can be estimated. The difference of these both values is given in Figure 15 exemplarily for six measurements. As the mechanical energy has to be extracted from the water circuit, the values of $\dot{Q}_{RD}$ exceeds the values of P_1. The lowest measured values refer to the measurement without solidification at standstill and amount to 50 W. As there is no mechanical energy dissipated into the system, this is the heat loss to the ambient. Thereby, the losses can be differed into losses at the rotating drum insulation and at the water circuit. The losses at the rotating drum can be determined with the data given in Figure 10 for no temperature difference $\Delta T_{PCM,l\text{-}HTF}$ between the HTF and the liquid PCM. The losses are increasing with the rotational speed from 7 W at 0 min^{-1} to 29 W at 25 min^{-1}. The additional losses have to be at the water circuit. With an increase of the rotational speed, the difference of the measured values given in Figure 15 increases also for no solidification. This increase is due to friction at the bare surface and the scraper and within the rotary bearings. Its maximum of 48 W can be found at 10 min^{-1} for the measurement with adhesion. When solidification occurs, the difference of the values to the heat loss of 50 W refers to both, the friction and the mechanical power needed for scraping off the solidified PCM. The average additional power is 44 W for a temperature configuration of 20K/5K/15K and 79 W for a temperature

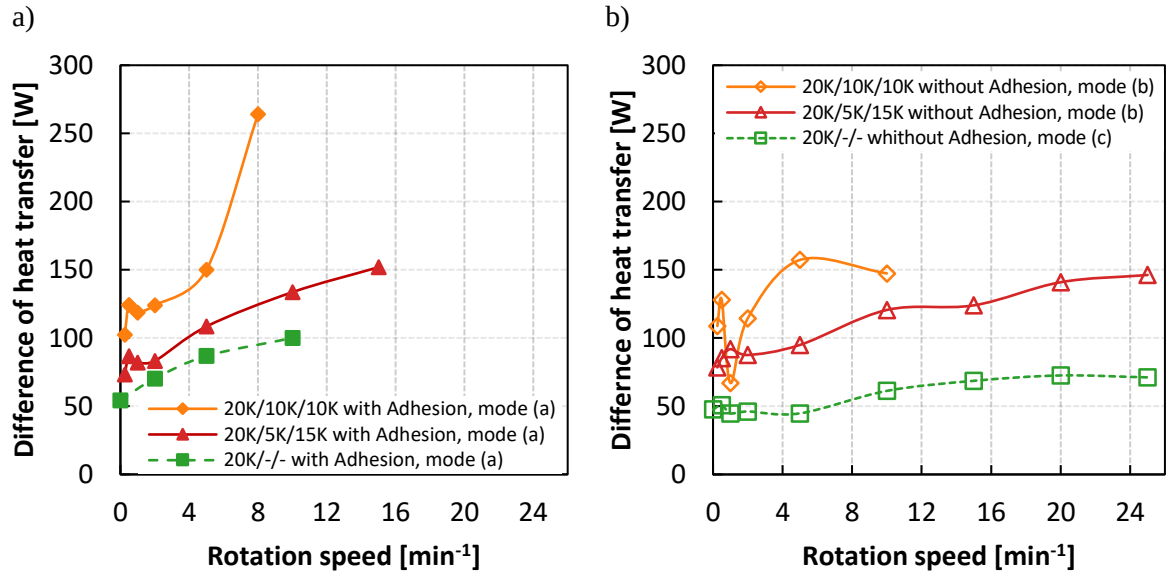

Figure 15: Difference between the measured electrical power P_1 and the thermal power determinate at the plate heat exchanger $\dot{Q}_{RD}$

configuration of 20K/10K/10K. For the measurements with adhesion, the increase is 17 % higher in average compared to the measurements without adhesion. The mechanical power due to friction and scraping off the solidified PCM increases with higher rotational speeds. The maximum mechanical power is 100 W for a temperature configuration of 20K/5K/15K and 215 W for a temperature configuration of 20K/10K/10K. When comparing the mechanical power due to friction and for scraping off the PCM from the drum surface with the thermal power, the value decreases with higher rotational speeds. Thus, the average mechanical power is 8 % of the thermal power at 5 min^{-1} and decreases below 5 % at 15 min^{-1}. Be aware that the experimental test rig is not optimized for low mechanical power consumption.

3.4 Heat transfer density at the rotating drum surface

By relating the measured heat transfer to a specific surface, the heat transfer potential can be compared with other heat exchange technologies. Since the active heat transfer surface is not clearly defined at the rotating drum, the measured heat transfer is related to the submerged drum shell surface and the total drum shell surface. The results are given Figure 16.When relating the measured heat transfer with adhesion to the submerged surface only, a heat transfer density of up to 28.8 kW/m^2 at a rotational speed of 15 min^{-1} is determined. Since the heat transfer surface is expanded by the adhesion to the surface outside the liquid PCM as well, the heat transfer density related to the total drum surface is more expressive. This results in a heat transfer density of up to 6.8 $kW \cdot m^{-2}$. When removing the liquid adhering layer with the rubber lip, the heat transfer density is 21 $kW \cdot m^{-2}$ at 15 min^{-1} and 25.8 $kW \cdot m^{-2}$ at 25 min^{-1} when relating the measured heat transfer to the submerged drum shell surface. When relating the measured heat transfer to the total drum shell surface, the heat transfer densities are 4.9 $kW \cdot m^{-2}$ and 6.1 $kW \cdot m^{-2}$. These values are for the specific experimental test rig. An optimized system will reach higher surface specific heat transfer rates as mentioned in section 4.

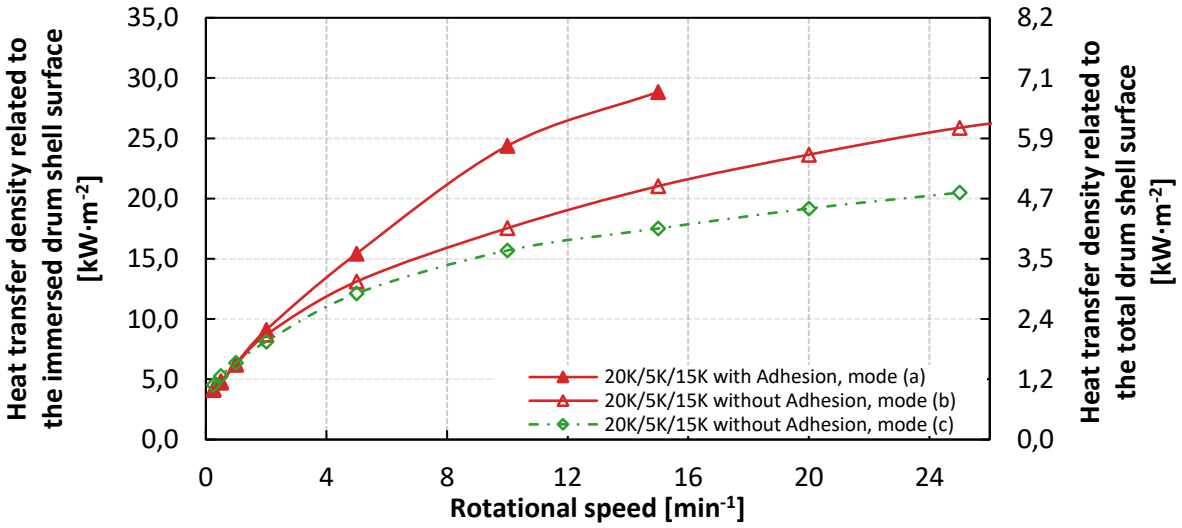

Figure 16: Heat transfer densities related to the immersed drum shell surface (left axis) and the total drum shell surface (right axis) at the rotating drum for a temperature configuration of 20K/15K/5K and a variation of the operation modes

4 Conclusion and outlook

In order to increase the predictability of steam generated from fluctuating renewable energy for industrial processes as well as for power plants, LHTES are particularly suitable due to the isothermal phase change during melting and solidification. The deliverable thermal power of all state-of-the-art passive LHTES is decreasing during the discharge process due to a growing insulation layer out of solidified PCM at the heat exchanger surface. Furthermore, passive LHTES have a fixed ratio between power and capacity as the amount of PCM is fixed to the size of the heat transfer structure. The introduced and experimentally demonstrated rotating drum heat exchanger for LHTES overcomes this limitation by a continuously scraped heat exchanger surface. The novelty compared to already known active LHTES concepts is the consistent minimization of the thickness of the solidified PCM layer. This

increases the heat transfer to a maximum. By changing the rotational speed, the thermal power output can be controlled. Thus, a specific characteristic curve of the thermal power output of the system in dependence of the rotational speed can be given. The commissioned experimental test rig using the low temperature PCM decanoic acid and water as HTF serves as a proof-of-concept. The scraper, made out of a metal sheet pressed against the drums surface, works smoothly.

The measured transferred heat is constant at consistent rotational speeds and temperature differences and can be increased by increasing the rotational speed. The measured heat transfer at the presented test rig is up to 1.6 kW for a total temperature difference between the HTF and the liquid PCM $\Delta T_{PCM,l\text{-}HTF}$ of 20 K. Compared to the heat transfer at pure forced convection without solidification, the heat transfer is up to 142 % higher when solidification occurs at a constant total temperature difference $\Delta T_{PCM,l\text{-}HTF}$ and constant rotational speed. During solidification, a rise of the temperature difference between the HTF and the melting point of the PCM $\Delta T_{PCM,m\text{-}HTF}$ by 5 K increases the transferred heat by 31 % in average while a rise of the temperature difference between the melting point of the PCM and the temperature of the liquid PCM $\Delta T_{PCM,l\text{-}PCM,m}$ increases the heat transfer by only 11 % in average. When the surface of the rotating drum emerges from the liquid PCM, liquid PCM adheres at the solidified layer. This increases the total heat transfer by up to 60 % as the liquid PCM solidifies after the surface emerged. The total measured layer thicknesses, composed out of a solidified part and an adhering part, decrease with higher rotational speeds. Thus, total layer thicknesses of below 0.05 mm can be achieved.

In a next step, an analytical and numerical scheme to investigate the un-steady effects and the adhesion will complement the experimental results. The authors are working on several models right now and will publish the results soon. The theoretical models will be validated with the presented experimental results. When using sodium nitrate as PCM and a temperature difference between the melting point of the PCM and evaporating water as heat transfer fluid of 50 K, first calculations with the model show heat transfer densities of above 100 $kW \cdot m^{-2}$ based on the total drum surface. Furthermore, the authors are planning an experimental test of the rotating drum heat exchanger with a thermal power of 100 kW. It will be integrated into an entire heat storage system using a high temperature PCM for the generation of steam.

CRediT authorship contribution statement

Jonas Tombrink: Conceptualization, Methodology, Investigation, Validation, Visualization, Writing - original draft. Henning Jockenhöfer: Conceptualization, Writing - review & editing. Dan Bauer: Conceptualization, Funding acquisition, Supervision, Writing - review & editing.

Declaration of Competing Interest

The authors declare that they have no known competing financial interests or personal relationships that could have appeared to influence the work reported in this paper.

Funding

This research did not receive any specific grant from funding agencies in the public, commercial, or not-for-profit sectors.

References

[1] Naegler T, Simon S, Klein M, Gils HC. Quantification of the European industrial heat demand by branch and temperature level. Int J Energ Res. 2015;39:2019-30. https://doi.org/10.1002/er.3436

[2] Jockenhöfer H, Steinmann W-D, Bauer D. Detailed numerical investigation of a pumped thermal energy storage with low temperature heat integration. Energy. 2018;145:665-76. https://doi.org/10.1016/j.energy.2017.12.087

[3] Bauer T, Laing D, Tamme R. Characterization of Sodium Nitrate as Phase Change Material. Int J Thermophys. 2012;33:91-104. https://doi.org/10.1007/s10765-011-1113-9

[4] Vogel J, Felbinger J, Johnson M. Natural convection in high temperature flat plate latent heat thermal energy. Appl Energ. 2016;184:184-96. https://doi.org/10.1016/j.apenergy.2016.10.001

[5] Zhang SQ, Pu L, Xu LL, Liu R, Li YZ. Melting performance analysis of phase change materials in different finned thermal energy storage. Appl Therm Eng. 2020;176:115425. https://doi.org/10.1016/j.applthermaleng.2020.115425

[6] Ma Z, Yang W-W, Yuan F, Jin B, He Y-L. Investigation on the thermal performance of a high-temperature latent heat storage system. Appl Therm Eng. 2017;122:579-92. https://doi.org/10.1016/j.applthermaleng.2017.04.085

[7] Johnson M, Vogel J, Hempel M, Hachmann B, Dengel A. Design of High Temperature Thermal Energy Storage for High Power Levels. Sustain Cities Soc. 2017;35:758-63. https://doi.org/10.1016/j.scs.2017.09.007

[8] Opolot M, Zhao C, Liu M, Mancin S, Bruno F, Hooman K. Influence of cascaded graphite foams on thermal performance of high temperature phase change material storage systems. Appl Therm Eng. 2020;180:115618. https://doi.org/10.1016/j.applthermaleng.2020.115618

[9] Lin W, Zhang W, Ling Z, Fang X, Zhang Z. Experimental study of the thermal performance of a novel plate type heat exchanger with phase change material. Appl Therm Eng. 2020;178:115630. https://doi.org/10.1016/j.applthermaleng.2020.115630

[10] Raul A, Jain M, Gaikwad S, K. Saha S. Modelling and experimental study of latent heat thermal energy storage with encapsulated PCMs for solar thermal applications. Appl Therm Eng. 2018;143:415-28. https://doi.org/10.1016/j.applthermaleng.2018.07.123

[11] Kibria MA, Anisur MR, Mahfuz MH, Saidur R, Metselaar IHSC. A review on thermophysical properties of nanoparticle dispersed phase change materials. Energ Convers Manage. 2015;95:69-89. https://doi.org/10.1016/j.enconman.2015.02.028

[12] Tariq LS, Ali HM, Akram MA, Janjua MM, Ahmadlouydarab M. Nanoparticles enhanced phase change materials (NePCMs)-A recent review. Appl Therm Eng. 2020;176:115305. https://doi.org/10.1016/j.applthermaleng.2020.115305

[13] Huang X, Zhu C, Lin Y, Fang G. Thermal properties and applications of microencapsulated PCM for thermal energy storage: A review. Appl Therm Eng. 2019;147:841-55. https://doi.org/10.1016/j.applthermaleng.2018.11.007

[14] Giro-Paloma J, Martinez M, F. Cabeza L, Fernandez AI. Types, methods, techniques, and applications for microencapsulated phase change materials (MPCM): A review. Renew Sust Energ Rev. 2016;53:1059-75. https://doi.org/10.1016/j.rser.2015.09.040

[15] Jiang Y, Liu M, Sun Y. Review on the development of high temperature phase change material composites for solar thermal energy storage. Sol Energ Mat Sol C. 2019;203:110164. https://doi.org/10.1016/j.solmat.2019.110164

[16] Tombrink J, Jockenhöfer H, Bauer D. Examination of the heat transfer potential of an active latent heat storage concept. Eurotherm Seminar nº112 - Advances in Thermal Energy Storage. Lleida 2019.

[17] Zipf V, Anton N, Daniel W, Peter N, Stefan G, Werner P. High temperature latent heat storage with a screw heat exchanger: Design of prototype. Appl Energ. 2013;109:462-9. https://doi.org/10.1016/j.apenergy.2012.11.044

[18] Pointner H, Steinmann W-D. Experimental demonstration of an active latent heat storage concept. Appl Energ. 2016;168:661-71. http://dx.doi.org/10.1016/j.apenergy.2016.01.113

[19] Nepustil U, Laing-Nepustil D, Lodemann D, Sivabalan R, Hausmann V. High Temperature Latent Heat Storage with Direct Electrical Charging – Second Generation Design. Energy Procedia. 2016;99:314-20. https://doi.org/10.1016/j.egypro.2016.10.121

[20] Maruoka N, Tsutsumi T, Ito A, Hayasaka M, Nogami H. Heat release characteristics of a latent heat storage heat exchanger by scraping the solidified phase change material layer. Energy. 2020;205:118055. https://doi.org/10.1016/j.energy.2020.118055

[21] Lakhdar MB, Cerecero R, Alvarez G, Guilpart J, Flick D, Lallemand A. Heat transfer with freezing in a scraped surface heat exchanger. Appl Therm Eng. 2005;25:45-60. https://doi.org/10.1016/j.applthermaleng.2004.05.007

[22] Saraceno L, Boccardi G, Celata GP, Lazzarini R, Trinchieri R. Development of two heat transfer correlations for a scraped surface heat exchanger in an ice-cream machine. Appl Therm Eng. 2011;31:4106-12. https://doi.org/10.1016/j.applthermaleng.2011.08.022

[23] Marizy C, Le Bail A, Duprat JC, Reverdy Y. Modelling of a drum freezer. Application to the freezing of mashed broccoli. J Food Eng. 1998;37:305-22. https://doi.org/10.1016/S0260-8774(98)00052-1

[24] Rao CS, Hartel RW. Scraped surface heat exchangers. Crit Rev Food Sci Nutr. 2006;46:207-19. https://doi.org/10.1080/10408390500315561

[25] VDI Heat Atlas. Berlin Heidelberg: Springer-Verlag; 2010.

[26] Nazir H, Batool M, Ali M, M. Kannan A. Fatty acids based eutectic phase change system for thermal energy storage applications. Appl Therm Eng. 2018;142:466-75. https://doi.org/10.1016/j.applthermaleng.2018.07.025

[27] Yuan Y, Zhang N, Tao W, Cao X, He Y. Fatty acids as phase change materials: A review. Renew Sust Energ Rev. 2014;29:482-98. https://doi.org/10.1016/j.rser.2013.08.107

[28] Kahwaji S, Johnson MB, Kheirabadi AC, Groulx D, White MA. Fatty acids and related phase change materials for reliable thermal energy storage at moderate temperatures. Sol Energ Mat Sol C. 2017;167:109-20. https://doi.org/10.1016/j.solmat.2017.03.038

[29] Abhat A. Low Temperature Latent Heat Thermal Energy Storage: Heat Storage Materials. Sol Energy. 1983;30:313-32. https://doi.org/10.1016/0038-092X(83)90186-X

[30] Noureddini H, Teoh BC, Clements LD. Densities of Vegetable Oils and Fatty Acids. J Am Oil Chem Soc. 1992;69:1184-8. https://doi.org/10.1007/BF02637677

[31] Noureddini H, Teoh BC, Clements LD. Viscosities of vegetable oils and fatty acids. J Am Oil Chem Soc. 1992;69:1189-91. https://doi.org/10.1007/BF02637678

[32] Rozanna D, Chuah TG, Salmiah A, Choong TSY, Sa'ari M. Fatty Acids as Phase Change Materials (PCMs) for Thermal Energy Storage: A Review. Int J Green Energy. 2004;1:495-513. https://doi.org/10.1081/GE-200038722

[33] Taylor JR. An Introduction to Error Analysis: The Study of Uncertainties in Physical Measurements. Sausalito, California: University Science Books; 1997.